Comparison of dynamical decoupling protocols for a nitrogen-vacancy center in diamond

Zhi-Hui Wang,[1] G. de Lange,[2] D. Ristè,[2] R. Hanson,[2] and V. V. Dobrovitski[1]

[1]*Ames Laboratory, Iowa State University, Ames, Iowa 50011, USA*
[2]*Kavli Institute of Nanoscience Delft, Delft University of Technology, P.O. Box 5046, NL-2600 GA Delft, The Netherlands*

We perform a detailed theoretical-experimental study of the dynamical decoupling (DD) of the nitrogen-vacancy (NV) center in diamond. We investigate the DD sequences applied to suppress the dephasing of the electron spin of the NV center induced by the coupling to a spin bath composed of the substitutional nitrogen atoms. The decoupling efficiency of various DD schemes is studied, including both periodic and aperiodic pulse sequences. For ideal control pulses, we find that the DD protocols with the Carr-Purcell-Meiboom-Gill (CPMG) timing of the pulses provides best performance. We show that, as the number of control pulses increases, the decoupling fidelity scaling differs qualitatively from the predictions of the Magnus expansion, and explain the origin of this difference. In particular, more advanced symmetrized or concatenated protocols do not improve the DD performance. Next, we investigate the impact of the systematic instrumental pulse errors in different periodic and aperiodic pulse sequences. The DD protocols with the single-axis control do not preserve all spin components in the presence of the pulse errors, and the two-axis control is needed. We demonstrate that the two-axis control sequence with the CPMG timing is very robust with respect to the pulse errors. The impact of the pulse errors can be diminished further by symmetrizing this protocol. For all protocols studied here, we present a detailed account of the pulse error parameters which make the strongest impact on the DD performance. In conclusion, we give specific recommendations about choosing the decoupling protocol for the system under investigation.

I. INTRODUCTION

A singly negatively charged nitrogen-vacancy (NV) center in diamond has recently emerged as a promising candidate for solid-state quantum computation and quantum information processing,[1–10] and high-precision electric and magnetic sensor for nanoscale applications.[11–20] The quantum state of the electron spin of a single NV center can be conveniently initialized and read out optically,[21–23] and coherently manipulated electrically, optically, and magnetically, even at room temperatures.[24–31] By prolonging the coherence time of the NV center spin, these favorable properties can be better exploited for potential applications.

Dynamical decoupling (DD) is an efficient tool for decoherence suppression. In nuclear magnetic resonance, the techniques based on Hahn spin echo, which employ the control pulses to manipulate the spins and achieve high-resolution spectra, have been widely used for several decades.[32] Lately, DD has been actively explored in the general context of QIP. By applying a sequence of control pulses (π rotations) to the qubit, in the limit of very short interpulse delay, DD can effectively cancel the coupling between the system and its decohering environment, thus preserving the qubit coherence.[33,34] Various DD schemes have been developed,[33–41] and implemented on different spin systems.[36,37,42–48]

DD has been recently implemented on single NV centers.[49–51] Excellent performance of several basic DD sequences has been demonstrated, thus opening the way to using DD in various experimental applications of NV centers. Understanding the performance of different DD schemes on NV centers in diamond is timely, and will be useful for future developments in this area of research. In this paper, we present a detailed study of various DD sequences designed to preserve the quantum state of a single NV center spin decohered by a spin bath of substitutional nitrogen defects (P1 centers), which

is the dominant decoherence source for the type Ib diamonds. We identify the most useful DD protocols, and study their efficiency in realistic experimental situations.

A large family of DD protocols is constructed based on the pulse sequences with periodic structure. Representatives are the Carr-Purcell-Meiboom-Gill (CPMG) sequence and its generalizations,[52,53] and periodic dynamical decoupling (PDD).[33,34,38,54] Among them, the sequences where all pulses rotate the spin about the same axis (single-axis control) refocus the spin dephasing, while the sequences where the spin is rotated alternatively about two mutually orthogonal axes (two-axis control) are able to suppress general decoherence.[34] However, the interpulse delay can never be made arbitrarily small to completely eliminate decoherence, because of unavoidable experimental constraints. These constraints limit the efficiency of the basic DD schemes. To suppress the effect of system-environment coupling more efficiently, more advanced symmetrized versions of periodic dynamical decoupling,[32,55] and the concatenated dynamical decoupling (CDD) have been proposed.[35,56]

Another important family of DD protocols is based on aperiodic DD schemes, such as Uhrig's DD (UDD), where the pulse spacings are optimized to suppress dephasing with a given number of pulses.[39] A DD scheme extending UDD to the two-axis control, the quadratic DD (QDD) has been proposed for suppression of general decoherence.[41] The performance of a given decoupling sequence strongly depends on the nature of the decohering bath. It has been demonstrated that for a bath with rapidly decaying spectral density, UDD performs better than periodic protocols (like CPMG) with the same number of pulses, while for a bath with a soft frequency cutoff in the spectral density, CPMG-like pulse spacing is preferred.[36,49,50,57–61] In a more general situation, the pulse positions can be numerically optimized for a given type of the bath.[36,37,62,63]

Here we consider the decohering bath made of the electron spins of P1 centers, which are coupled to the NV center and to each other via long-range dipolar coupling. The effect of such a bath is accurately approximated by the mean-field model of a random magnetic field acting on the NV center and leading to the dephasing of the NV spin.[25,49] We perform theoretical and experimental study of DD in such a system, studying both periodic and aperiodic DD sequences based on single- and two-axis control, as well as their symmetrized and concatenated versions. Using both analytical and numerical tools, we show that the periodic sequences with equally spaced pulses (PDD) and the sequences with CPMG timing exhibit different short and long time behavior. The aperiodical sequences UDD and QDD show inferior performance in comparison with the CPMG-timed sequences, in accordance with the previous studies mentioned above. We further demonstrate that, in contrast with the expectations, the concatenated DD sequences do not improve the performance of decoupling; we clarify the origin of this behavior.

For ideal DD pulses, the decoupling efficiency grows in the limit of very short inter-pulse delay (in nonpathological cases). On the other hand, as the number of DD pulses is increased to achieve shorter delay, the negative effect of the unavoidable imperfections in the control pulses becomes noticeable. At long times, the pulse error accumulation can completely destroy the DD performance,[52,64] and understanding the impact of the pulse errors is important for successful decoupling. Below, we focus on the instrumental pulse errors caused by imperfect adjustment of the rotation axis/angle (the errors caused by decoherence during the control pulse are much less important in our experiments). Since the 1970s, a vast number of recipes has been suggested to reduce the effect of the instrumental pulse errors, from pulse tuning and shaping minimizing the individual pulse errors,[65–72] to combining the imperfect pulses in order to compensate the errors.[55,73–75] In our work, minimization of the errors is not addressed: We assume them fixed. We analyze how different sequences accumulate or compensate these fixed instrumental pulse errors: This is known to drastically depend on the specific sequence.[35,36,44,56,61,62,76–78] We show that the CPMG and the UDD sequences accumulate pulse errors in the rotation angle and the z component of the rotation axis, with the decoupling fidelity being sensitive to the initial spin state. The sequences based on the two-axis control are in general more robust to the pulse errors; we provide a detailed account of the most important components of the pulse errors. As a result, our results provide a detailed understanding of the dynamical decoupling of a single NV center spin in the bath of P1 centers in diamond.

The rest of this paper is organized as follows: In Sec. II we describe the system under study, an NV center in diamond. Section III presents description of the experiments. In Sec. IV we analyze the decoupling performance of the DD protocols assuming ideal pulses. In Sec. V we focus on the accumulation of pulse errors in various DD sequences for different states of the NV center's spin. In Sec. VI we discuss the internal structure of the bath under study. Conclusions are given in Sec. VII.

II. DESCRIPTION OF THE SYSTEM: AN NV CENTER IN DIAMOND

The singly negatively charged NV center in diamond is composed of a vacancy defect and an adjacent substitutional nitrogen atom. The electronic ground state of the center has a total spin $S = 1$ with a zero-field splitting $D = 2.87$ GHz between the $m_S = 0$ and $m_S = \pm 1$ levels.[79] The quantization axis of this splitting is along the symmetry axis of the NV center, which we take as the z axis. In our experiments, a static magnetic field $B_0 = 114$ G is applied along the z axis, and the sublevels $m_S = +1$ and $m_S = -1$ are separated. The transition energies between states $m_S = 0$ and $m_S = +1$ and that between $m_S = 0$ and $m_S = -1$ differ by hundreds of MHz. We apply pulses to the NV center only in resonance with the transition between $m_S = 0$ and $m_S = -1$, which can thus be regarded as an effective two-level system $S_0 = 1/2$ (the central spin). The NV center spin is coupled to the nuclear spin of the host nitrogen atom I_0 via hyperfine interaction $A_0 S_0^z I_0^z$, where $A_0 = -2\pi \times 2.16$ MHz for ^{14}N, and $A_0 = 2\pi \times 3.03$ MHz for ^{15}N nuclei, respectively.[80] The intrinsic relaxation time of the nuclear spin is of orders of milliseconds, so that I_0 for a single experimental run is a constant of motion which merely shifts the Larmor frequency of the NV center spin, but changes from one run to another.

The NV center is surrounded by a large number of P1 centers (abundance ~ 0.02 % in our sample), which form the decohering bath. Each P1 center is composed of an unpaired electron with spin $S_k = 1/2$ and a ^{14}N nuclear spin $I_k = 1$, coupled via hyperfine interaction of the order of 100 MHz. The NV center spin S_0 is dipolarly coupled to all S_k with the coupling strength ~ 1 MHz, and the dipolar coupling between the electron spins of different P1 centers is also of order of 1 MHz. The dipolar interactions between different spins S_k, therefore, are responsible for the internal dynamics of the spin bath, leading to the flip-flops between different bath spins. At the same time, the flip-flops between the central spin S_0 and the bath spins S_k are strongly suppressed, due to the large mismatch in the transition energies (2.55 GHz for the NV center spin vs a few hundreds of MHz for a P1 center). Therefore, decoherence of the NV center spin is dominated by pure dephasing [i.e., decay of the transversal (the x-y plane) component of the NV spin]. The longitudinal z component, which decays at much longer times (tens of milliseconds and up, mostly due to spin-phonon relaxation), is assumed to be conserved. In this situation, the bath of P1 centers can be represented[25,49] as a bath of spins $1/2$ (which we denote as $\tilde{S}_k$), with the system-bath coupling Hamiltonian,

$$H_{\text{SB}} = S_0^z \sum_k a_k \tilde{S}_k^z. \tag{1}$$

Each coupling constants a_k depends on the specific state of the nuclear spin of the kth P1 center, on the direction of the symmetry axis of this P1 center, and on the location of this P1 center with respect to the NV center. For details, see Sec. VI below, and the supporting material of Ref. 25.

The decoherence problem for a central spin coupled to a many-spin bath is typically beyond the reach of analytical treatment due to the complex intrabath dynamics. Many methods have been developed in the field of magnetic

resonance,[81–84] and recently in the field of quantum information processing.[4,25,59,60,85–95]

In this work, we treat the spin bath of P1 centers in a mean-field manner, approximating it as a classical noise field acting on the NV center spin. This treatment is justified because the coupling between the bath spins is of long-range character, and its magnitude is of the same order as the coupling of a bath spin to the central spin. In this case, the back-action from the central spin on the bath is negligible: The action of a single NV center on a given P1 spin is small in comparison with the action of hundreds of other bath spins. Next, due to the long-range character of the dipolar coupling, the NV spin experiences the action of a large number of P1 bath spins. As a result, the action of the bath as a whole on the NV spin can be approximated as a random magnetic field, which is Gaussian (due to the large number of bath spins acting on the NV spin with comparable strength), has zero mean, and whose variance is[96] $b^2 = (1/4) \sum_k a_k^2$. Due to small back-action, this random field is stationary. Moreover, since each bath spin is coupled to a large number of other bath spins, and the dynamics of different bath spins are incoherent, we expect this random magnetic field to be Markovian (i.e., history independent).

This treatment follows the lines of the early works in the area of magnetic resonance.[81–83] It has been numerically and experimentally justified for the system under consideration.[25,49,85,88] We stress that the validity of such approximation is built upon the assumption of small back-action from the central spin and the lack of coherence between the dynamics of different bath spins. If the couplings between the bath spins are much smaller than the coupling between a single bath spin and the central spin, then the bath dynamics is conditioned on the state of the central spin, and the resulting correlations in the bath play a major role.[60,87,89–91,95]

The noise field $B(t)$, which is Gaussian, Markovian, and stationary, is represented by an Ornstein-Uhlenbeck (O-U) process[97] with the correlation function,

$$C(t) = \langle B(0)B(t) \rangle = b^2 \exp(-|t|/\tau_c), \quad (2)$$

where b describes the characteristic coupling strength of the central spin to the bath, and τ_c is the correlation time of the noise field (governed by the coupling between the bath spins). Thus, the Hamiltonian governing the dynamics of the central spin is

$$H = S_0^z B_1(t) + H_c(t), \quad (3)$$

where the term $H_c(t)$ represents the control pulses (specified below), and the field $B_1(t)$ includes the random bath field $B(t)$, the static applied field, and the hyperfine field $A_0 I_0^z$ from the NV's own nuclear spin. Here and below we adopt the unit $\hbar = \gamma = 1$, where γ is the gyromagnetic ratio for the NV center spin.

The performance of a DD sequence can be measured by the overlap between the initial state and the state after the pulse sequence, $\mathrm{Tr}[\rho(0)\rho_S(t)]$, where $\rho(0) = |\psi(0)\rangle\langle\psi(0)|$ is the initial density matrix of the central spin, and $\rho_S(t)$ is the reduced density matrix of the central spin at time t; we assume that the central spin is disentangled from the bath at $t = 0$ and is prepared in the pure state $|\psi(0)\rangle$. In our study, we focus on two initial states of the central spin, with the spin directed along the x and the y axes, which we will denote as $|X\rangle$ and

$|Y\rangle$, respectively. Any density matrix for a spin-1/2 system can be expressed as

$$\rho_S(t) = (1/2)[\mathbf{1} + S_X \sigma_x + S_Y \sigma_y + S_Z \sigma_z], \quad (4)$$

where $\mathbf{1}$ is the identity operator, $\sigma_{x,y,z}$ are the Pauli operators, and the parameters $S_{X,Y,Z}$ determine the corresponding spin projections. Below, we use these parameters to characterize the decoupling fidelity: They are directly related to the standard fidelity measure,[98] which in our setting acquires the form $F = \sqrt{\langle\psi(0)|\rho_S(t)|\psi(0)\rangle}$. The fidelities S_X and S_Y are normalized to the range $[-1,1]$, are directly determined experimentally, and coincide with $2F^2 - 1$ for the corresponding initial states.

Our analysis and numerical simulations have been performed in a rotating frame with a frequency close to the center of the ESR line of the NV center spin. In this rotating frame, the average field $\langle B_1(t) \rangle$ is $B_{\mathtt{dtn}} + A_0 I_0^z$, where $B_{\mathtt{dtn}}$ is the small detuning of the pulse field from the exact resonance. Its value $B_{\mathtt{dtn}} = -2\pi \times 0.5\,\mathrm{MHz}$ has been obtained by fitting the experimental results. In simulations, for different realizations of $B(t)$, we randomly sample the values of $I_0^z = +1, -1, 0$ with the probabilities $p_+ = 0.5$, $p_- = 0.2$, $p_0 = 0.3$, respectively. These values are determined experimentally, from the Ramsey fringe experiments.

III. EXPERIMENTAL SETUP

We study NV centers in a Ib bulk diamond sample (Element Six) which is mounted in a scanning confocal microscope at room temperature.[29] The local density of electronic spins surrounding the NV center used in these experiments is $\sim$100 ppm, which is estimated from the decay of Ramsey fringes of nitrogen spins.[99] A static magnetic field ($B_0 = 114$ G) is applied along the NV symmetry axis by a custom-made vector magnet (Alpha Magnetics).

The envelopes of the pulse sequences are generated using an arbitrary wave-form generator (Tektronix AWG 5014B). The AWG is connected to the I/Q modulation inputs of a vector signal generator (R&S SMBV100A) which has a 250-MHz modulation bandwidth. In order to achieve high Rabi frequencies we amplify the microwave signal using a high-power amplifier (AR 25S1G4). The amplified signal is delivered to the sample by a coplanar waveguide (CPW) which is fabricated directly on the surface of the diamond.[27,49] This configuration allows us to generate sequences with short (8-ns) π pulses with arbitrary but well-defined relative phases.

IV. DYNAMICAL DECOUPLING WITH IDEAL PULSES

Analysis of DD is often based on the Magnus expansion (ME),[32] which is a cumulant expansion of the evolution operator of the system. However, the Magnus expansion is not always sufficient for the analysis of DD under realistic conditions. As an asymptotic expansion, the ME is valid only for the sequences with very short period, satisfying the condition $T_c||H_B|| \ll 1$, where T_c is the DD period, and $||H_B||$ is the norm of the bath Hamiltonian. In many realistic situations, $||H_B||$ is macroscopically large, and the formal ME validity condition requires unreasonably small T_c; nevertheless, DD performs very well far beyond the formal ME limits. In this work, by virtue of the known properties of

the O-U process, we perform analytical and numerical study of different DD sequences without invoking ME.

Specifically, we study the following protocols: PDD XY (in which the central spin is rotated about the x and y axes alternately), its symmetrized version SDD XY and concatenated CDD versions; CPMG, XY4 (a DD scheme with the same timing as CPMG but based on the two-axis control),[53] its symmetrized version XY8 and its concatenated version CDD^{XY4}. We also consider the aperiodic UDD sequence and its extension QDD.[41]

In this section, we assume the pulses in the DD sequences are ideal (i.e., without pulse errors), and focus on the performance of DD sequences as a function of the interpulse delay. Note that for ideal pulses, in the regime of pure dephasing, the axes of the π pulses in the DD sequence are irrelevant, as explained below. Thus, our results are equally applicable to the case of the single-axis control sequences (single-axis PDD, SDD, CDD, etc.) However, as we will see in the subsequent sections, the single-axis protocols perform poorly in the case of nonideal pulses, so these protocols are of secondary importance for our purposes.

A. Analytical expression for decoherence

The dephasing dynamics of a spin 1/2 subjected to a classical O-U noise field $B(t)$ can be studied analytically. The transverse spin component precesses around the z axis, and is rotated by an angle $\Phi(T) = \int_0^T B(t)dt$ at time $t = T$, so that the spin components along x and y are determined by $\langle \cos \Phi(T) \rangle$ and $\langle \sin \Phi(T) \rangle$, where the angular brackets denote the averaging over all realizations of the O-U process. Note that in this section, the static detuning B_{dtn} and the static hyperfine field are neglected: For perfect DD pulses, these static fields are completely removed by a single-pulse spin echo, and by any DD sequence.

For an O-U process with zero mean, $\langle \sin \Phi \rangle = 0$, so that the decoherence leads only to the decay of the initial spin component, without extra rotation, that is, if the central spin was prepared at $t = 0$ along the x axis ($S_X = 1$, and $S_Y = S_Z = 0$), then $S_Y = S_Z = 0$ at all times, while

$$S_X(T) = F(T) = \left\langle \exp\left(-i \int_0^T B(t)dt\right) \right\rangle. \quad (5)$$

The decay function $F(T)$ in the case of free evolution (no DD pulses) can be easily calculated:[81,82] The transition probability for a O-U process has Gaussian form, so the functional in the equation above is a standard Gaussian path integral. For a slowly fluctuating bath, with $b\tau_c \gg 1$, the free decay of the central spin has Gaussian form $F(T) = \exp(-b^2 T^2/2)$.

In a spin echo experiment, after free evolution during time τ, a π pulse is applied, flipping the sign of the z component of the central spin, and the sign of the phase accumulation is inverted. The resulting change in the dynamics can be described by correspondingly rotating the coordinate frame and inverting the sign of the field $B(t)$.[32,52] Thus, for a single-pulse Hahn echo experiment, of total duration $T = 2\tau$, the decay of the transversal component of the central spin is determined by the functional[81] $E(2\tau) = \langle \exp(-i \int_0^\tau B(t)dt + i \int_\tau^{2\tau} B(t)dt) \rangle$. This is another Gaussian path integral which can be calculated explicitly, and for a slow

bath ($b\tau_c \gg 1$) has a form $E(T = 2\tau) = \exp(-T/T_2)^3$, where the echo decay time,

$$T_2 = \left(\frac{12\tau_c}{b^2}\right)^{1/3}. \quad (6)$$

Our experiments on the Ramsey fringes decay (measuring the free dephasing rate) and on the Hahn spin echo decay demonstrate the theoretically predicted behavior. The measurements of the free decay time ($T_2^* = 0.4 \mu s$) and the echo decay time ($T_2 = 2.8 \mu s$) allow one to determine the bath parameters:

$$\begin{aligned} \tau_c &= 25 \ \mu s \\ b &= 3.6 \ \mu s^{-1}. \end{aligned} \quad (7)$$

These values agree with the parameters measured later in Ref. 99. The EPR measurements, performed on a macroscopic ensemble of NV centers, cannot be used to extract the value of b for a single NV center:[88] Even in a macroscopically homogeneous sample, the distribution of b for different NV centers is very broad (has a heavy power-law tail), and the width of the EPR line can serve only as a crude order-of-magnitude estimate for some "typical" (in a loose sense) NV center. With this precaution, we note that the value of b given above is compatible with the nominal concentration of P1 centers (200 ppm), which is directly related to their EPR linewidth.[100]

When the central spin is subjected to a DD sequence, multiple π pulses are applied sequentially, and each pulse inverts the sign of S_0^z. As for the spin echo, the spin evolution is conveniently described in the toggling coordinate frame, which is rotated along with each spin rotation; correspondingly, the sign of the field $B(t)$ is inverted with each pulse.[32] Transforming the spin evolution in the toggling frame back to the standard rotating frame is not difficult: For ideal pulse it is enough to note that the two coordinate frames coincide at the end of every DD period. The spin evolution in this toggling coordinate frame remains essentially the same: The spin rotates in the x-y plane, and the total rotation angle is $\tilde{\Phi} = \int_0^T \xi(t)B(t)dt$, where $\xi(t)$ is the time-domain filter function, which takes into account the impact of the pulses: $\xi(0) = +1$, and changes sign every time when a π pulse is applied to the central spin.

Again, for an O-U process with zero mean, the decoherence in the presence of the DD pulses is reduced to the decay of the transverse spin component, without extra rotation. Considering the evolution of the central spin during the time interval $[0,T]$, the decoupling fidelity (equal to the transverse spin component) is

$$S(T) = \left\langle \exp\left(-i \int_0^T \xi(s)B(s)ds\right) \right\rangle, \quad (8)$$

where we omitted the index of the transverse component as irrelevant. For an O-U process $B(t)$, the averaging in Eq. (8) can then be carried out explicitly:[82] This is the characteristic functional of an O-U process, which can be rewritten in the form,

$$S(T) = \exp\left[-b^2 \int_0^T e^{-Rs} p(s)ds\right] = \exp[-b^2 W(T)], \quad (9)$$

where $R \equiv 1/\tau_c$, and the convolution integral $p(s) = \int_0^{T-s} \xi(t)\xi(t+s)dt$ contains all relevant information about the pulse sequence.

We consider a decoupling sequence containing N_c cycles, each of duration T_c, so that $T = N_c T_c$. In this case, it is convenient to define a filter function $\xi_0(t)$ for a single period: This function is zero at $t < 0$, equal to $+1$ at $t = 0$, changes sign every time a pulse is applied, and becomes zero at $t > T_c$. Then, the total function $\xi(t)$ for the kth cycle equals to $\xi_0(t - (k-1)T_c)$, and $\xi_0(t)$ therefore fully characterizes the pulse sequence. By calculating $p(s)$ in each cycle, and taking advantage of the periodicity of the sequence, the fidelity decay can be derived as

$$W(T) = \Gamma_N(Q_{11} + Q_{12}) - P_N Q_{12}, \qquad (10)$$

where Γ_N and P_N are N_c dependent constants given in Eq. (A7) in Appendix A and the integrals,

$$Q_{11} = \int_0^{T_c} e^{-Rs} q_{11}(s)ds,$$
$$Q_{12} = \int_0^{T_c} e^{-Rs} q_{11}(T_c - s)ds, \qquad (11)$$

with $q_{11}(s) = \int_0^{T_c-s} \xi_0(t)\xi_0(t+s)dt$. See Appendix A for the details of the derivation.

For any DD sequence with a periodical structure, it is then straightforward to calculate the decay of the decoupling fidelity, Eq. (10), starting from the specific filter function, $\xi_0(t)$.

Note that in the above derivation, since we are dealing with pure dephasing and ideal pulses, the axes of the π pulses in the DD sequence do not show up in the filter function. Therefore a π pulse about the x axis (denoted as π_X) and that about the y axis (π_Y) result in the same decoupling performance. It is the timing of the pulses that matters.

B. DD protocols based on equidistant pulses

We now study the performance of PDD XY, its concatenated version CDD, and its symmetrized version, SDD XY. While the results here are equally applicable to the corresponding single-axis protocols, the two-axis control is the main focus of our study.

Within the PDD XY protocol, the sequence of pulses d-π_X-d-π_Y-d-π_X-d-π_Y is repeated many times, where d denotes a free evolution of duration τ. Following the procedure in Sec. IV A, we can derive the dephasing exponent $W_{\text{PDD}}(t)$. In our experiments, the typical interpulse delay is ~ 0.02–1 μs, which is much shorter than the bath correlation time, $\tau_c = 25$ μs. We thus focus on the case $R\tau \ll 1$. When the number of cycles N_c is small, $RT = N_c R T_c \ll 1$ (we will refer to this regime as short times), the decoupling fidelity decays as

$$S(T) = \exp\left[-\frac{4}{N_d^2}\left(\frac{T}{T_2}\right)^3 \right], \qquad (12)$$

where T_2 is the spin echo decay time, Eq. (6), and N_d is the total number of the inter-pulse delays (equal to the total number of pulses). When N_c becomes so large that $RT = RN_c T_c \gg 1$ (we refer to this regime as long times), the decay rate becomes
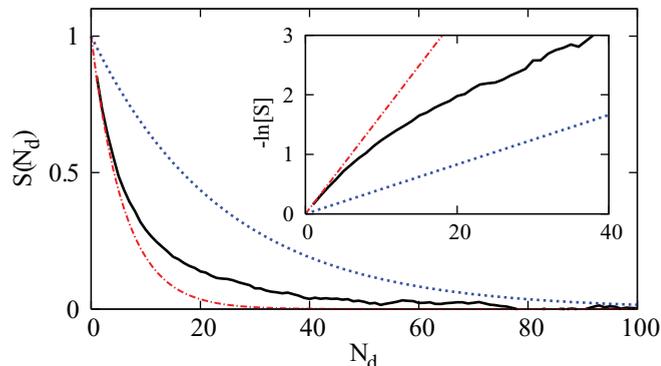
FIG. 1. (Color online) Simulation results for the decoupling fidelity as a function of the number N_d of the interpulse delays in PDD XY (solid black line). The dashed red line corresponds to the analytical expression (12) for small N_d, and the dotted blue line corresponds to the expression (13) for large N_d. The duration of the inter-pulse delay is $\tau = 0.6$ μs. The inset shows the same curves with logarithmic scale in the vertical axis, demonstrating that the solid black line (simulation results) is parallel to the dotted blue line (analytics for long times) after $N_d \sim 20$ [i.e., the decoherence rate corresponds to the long-time regime, Eq. (13)].

four times smaller:

$$S(T) = \exp\left[-\frac{1}{N_d^2}\left(\frac{T}{T_2}\right)^3 \right]. \qquad (13)$$

Thus, for PDD XY, as the number of period increases, the decay slows down (detailed derivation is in Appendix A 1). This feature is shown in Fig. 1, where numerical results for $S(t)$ are shown as a function of N_d, with fixed interpulse delay τ.

We now consider concatenated protocols based on PDD XY. The concatenated sequence of level ℓ, which we denote as CDD_ℓ, is constructed recursively as[35,56]

$$(\text{CDD}_{\ell-1}) - \pi_X - (\text{CDD}_{\ell-1}) - \pi_Y - (\text{CDD}_{\ell-1}) - \pi_X$$
$$-(\text{CDD}_{\ell-1}) - \pi_Y, \qquad (14)$$

starting from PDD XY as the first-level CDD sequence. Extension to larger times can be achieved either by increasing the concatenation level, or by periodically repeating CDD of a fixed level, since the length of the CDD period T_c increases exponentially with ℓ. The detailed analysis of this family of protocols is given in Appendix A 1: It is performed recursively, and the decay rate for CDD_ℓ can be calculated from that of $\text{CDD}_{\ell-1}$. In the most experimentally relevant case, when $RT_c \ll 1$, we find that for all concatenation levels, the decay rate for both short times and long times are the same, equal to the short-time decay rate of PDD XY, Eq. (12). This behavior is exactly the opposite of a general expectation based on ME, that by increasing the CDD order, the decoupling performance should improve. The origin of such discrepancy is presented later in Sec. IV C.

The symmetrized protocol, SDD XY, is constructed by taking the PDD XY period, and adding to it the time-inverted PDD XY period, producing the sequence with the period,

$$(\text{d-}\pi_X\text{-d-}\pi_Y\text{-d-}\pi_X\text{-d-}\pi_Y)\text{-}(\pi_Y\text{-d-}\pi_X\text{-d-}\pi_Y\text{-d-}\pi_X\text{-d}), \qquad (15)$$
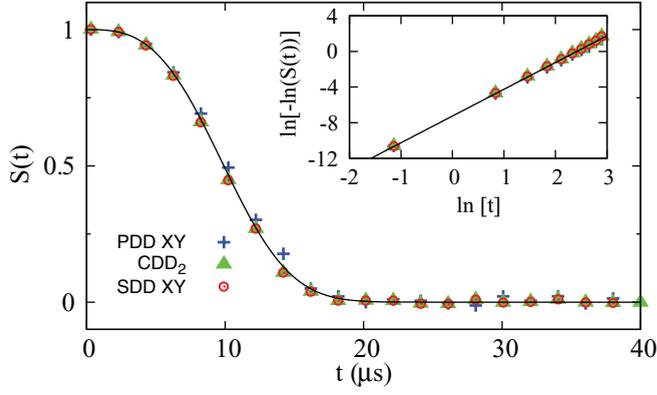
FIG. 2. (Color online) Simulation results for the decoupling fidelity as a function of the total evolution time for PDD XY (blue crosses), CDD$_2$ (green triangles), and SDD XY (red circles). In all protocols $N_d = 16$, and τ is increasing with t. The two latter sequences produce identical results. The black line shows the analytical results, Eq. (12). Inset shows the same results in log-log scale.

FIG. 3. (Color online) Decoupling fidelity as a function of the total evolution time. (a) XY4 for $N_d = 8, 16$ and 32 (red, green, and blue lines and symbols, correspondingly). Solid lines are analytical results obtained from Eq. (17), the dashed lines are numerical results, and the symbols are the experimental data. (b) Numerical results for XY4 with eight periods (red squares), CDD$_2^{\text{XY4}}$ (green circles), and XY8 (blue triangles) protocols with four periods. The number of delays is 64 for all protocols. The black line shows the analytical prediction of Eq. (17). As predicted, all three sequences demonstrate the same performance.

which has exactly the same timing of the pulses as the half-period of CDD$_2$ (since for ideal pulses $\pi_Y \pi_Y = \mathbf{1}$). The filter function for SDD XY therefore coincides with the filter function of CDD$_2$, and so is the decoupling fidelity. Figure 2 shows the numerical results for the performance of PDD XY, CDD$_2$, and SDD XY, each with $N_d = 16$. All curves agree with the analytical expression Eq. (12).

C. Sequences based on CPMG timing

The period of the CPMG sequence is d-π-d-d-π-d. The sequence XY4 has the same pulse timing, but is based on the two-axis control:[53]

$$\text{d-}\pi_X\text{-d-d-}\pi_Y\text{-d-d-}\pi_X\text{-d-d-}\pi_Y\text{-d.} \qquad (16)$$

Since we are considering ideal pulses, and limited to dephasing of the central spin, these two sequences are equivalent. Detailed analysis (in Appendix A 2) shows that the decay rate of the fidelity for both short and long times is the same. If we denote $T_{1/e}$ as the $1/e$ decay time of the decoupling fidelity, then for a sequence with CPMG timing, the fidelity decays as

$$S(T) = \exp\left[-\left(\frac{T}{T_{1/e}}\right)^3\right], \qquad (17)$$

with

$$T_{1/e} = \left(\frac{N_d}{2}\right)^{2/3} T_2. \qquad (18)$$

This is exactly the scaling behavior of the decay time observed in our experiments. Figure 3(a) shows the experimental data and the simulation results for $N_d = 8, 16, 32$, which are in excellent agreement with Eq. (17).

Let us compare XY4 with PDD XY. If we take the interpulse delays $\tau_{\text{PDD}} = 2\tau_{\text{XY4}}$, then the only difference between the two sequences will be the very first and the very last segments, each of duration τ_{XY4}. Equation (17) is then equivalent to Eq. (13), taking into account that $2N_d^{\text{PDD}} = N_d^{\text{XY4}}$. Therefore, at short times, the decay for the PDD XY sequence is four times faster

than for XY4. Note that this difference is the result of only two segments at the very beginning and at the very end of the sequence. For long times (large N_d), the decay rates of PDD XY and XY4 are the same, but the absolute value of the DD fidelity is exponentially higher for the CPMG-timed sequence XY4.

The symmetrized version of the XY4 sequence, often referred to as XY8,[53] has a period,

$$(\text{d-}\pi_X\text{-d-d-}\pi_Y\text{-d-d-}\pi_X\text{-d-d-}\pi_Y\text{-d})$$
$$-(\text{d-}\pi_Y\text{-d-d-}\pi_X\text{-d-d-}\pi_Y\text{-d-d-}\pi_X\text{-d}). \qquad (19)$$

Since its filter function is the same as XY4, the fidelity decay is also the same. For the concatenated version of XY4, the short-time and long-time decay rates in CDD$_\ell^{\text{XY4}}$ for any level are the same, equal to that in XY4 (see Appendix A 2). Figure 3(b) shows the simulation results for XY4, XY8, and CDD$_2^{\text{XY4}}$. The number of delays in all sequences is the same: $N_d = 64$ and the results are in agreement with Eq. (17).

Therefore, we arrive at the conclusion that for the spin bath considered in our study (Gaussian Markovian noise field with the Lorentzian spectrum), the performance of both the PDD- and the CPMG-based sequences is not improved neither by symmetrization or concatenation, and the simple XY4 sequence provides the optimal choice for experiments. This result may look somewhat discouraging, and is in contrast with the standard qualitative expectation, based on the Magnus expansion, that the higher-order sequences should generally provide better fidelity. It is also in clear contrast with the ME prediction that the decay exponent $W(T)$ for symmetrized sequences should contain only even-order terms, while our calculations produce $W(T) \sim T^3$. The problem here is the inapplicability of the Magnus expansion. The spectral density of our spin bath has a Lorentzian shape, $\sim 1/(R^2 + \omega^2)$, which has a formally infinite second moment. In terms of Magnus expansion, this corresponds to a formally infinite $||H_B||$. In reality, of course, the power spectrum of the spin bath is limited by the fastest possible flip-flop rate between two bath spins,

which is achieved when the two P1 centers are located at the nearest sites in the diamond lattice, but this frequency is in the GHz range, and is far above all other time scales relevant for decoherence. This situation is in sharp contrast with, for example, decoherence of the electron spin by a bath of nuclear spins in quantum dots.[59,60,87,90,92–95]

D. Aperiodic decoupling sequences

In the Uhrig DD scheme of level ℓ, denoted as UDD_ℓ, a sequence of π pulses rotate the spin about the same axis (taken here as x), and the pulses are applied at times,

$$t_j = T \sin^2 \left(\frac{j\pi}{2N_p + 2} \right), \tag{20}$$

where T is the total evolution time, and $j = 1, 2, \ldots, \ell$ for even ℓ and $j = 1, 2, \ldots, \ell + 1$ for odd ℓ. The generalization of the UDD for the case of the two-axis control, the QDD sequence,[41] is composed of two nested UDD sequences, during which the central spin is rotated about two perpendicular axes, respectively; to be concrete, here we consider the QDD sequence with π_X pulses in the outer hierarchical level, and π_Y pulses in the inner hierarchical level. Thus, for odd level $\ell = 2n - 1$, the QDD_ℓ sequence is

$$UDD_\ell^{(Y)}(\tau_1)\text{-}\pi_X\text{-}UDD_\ell^{(Y)}(\tau_2)\text{-}\pi_X\cdots\text{-}UDD_\ell^{(Y)}(\tau_{\ell+1})\text{-}\pi_X, \tag{21}$$

where $\sum_{j=1}^{\ell+1} \tau_j = T$ and $UDD_\ell^{(Y)}(\tau_j)$ denotes UDD_ℓ based on π_Y pulses with evolution time τ_j. The division of the total time T into intervals τ_j satisfies the same rule as for UDD (i.e., $\tau_j = t_j - t_{j-1}$), with t_j given by Eq. (20). The number of pulses in such a QDD sequence is $N_p = (\ell + 1)(\ell + 2)$. For even level $\ell = 2n$, the QDD_ℓ sequence is

$$UDD_\ell^{(Y)}(\tau_1)\text{-}\pi_X\text{-}\cdots\text{-}UDD_\ell^{(Y)}(\tau_\ell)\text{-}\pi_X\text{-}UDD_\ell^{(Y)}(\tau_{\ell+1}), \tag{22}$$

and the number of pulses is $N_p = \ell(\ell + 2)$.

The analysis in Sec. IV A is not applicable to UDD and QDD due to the lack of periodicity in these sequences. We perform only numerical study on these two sequences. Figure 4 shows the decoupling performance of UDD, in comparison with XY4 with the same number of pulses, $N_p = 8, 16$. For
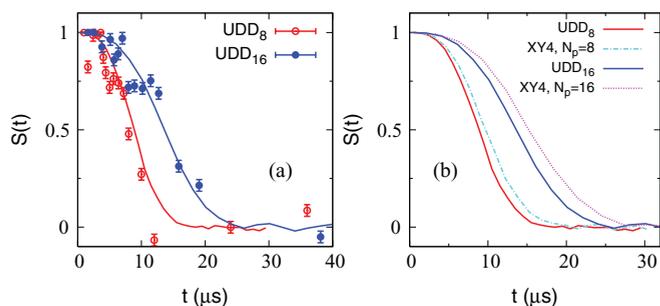
FIG. 4. (Color online) (a) Decoupling fidelity as a function of the total evolution time for UDD with $N_p = 8$ and $N_p = 16$ pulses (red and blue, respectively). Dots are the experimental data, and lines are simulation results. (b) Comparison of the simulation results for UDD (solid lines) and XY4 sequence (dashed lines) with the same number of pulses (red for $N_p = 8$ and blue for $N_p = 16$).
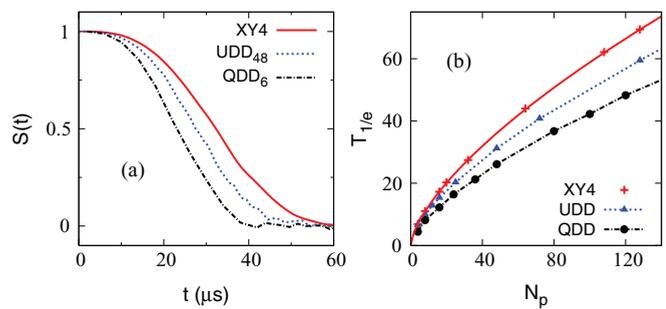
FIG. 5. (Color online) Simulation results. (a) Decoupling fidelity as a function of the total evolution time for XY4 with 12 periods, UDD_{48}, and QDD_6. Each sequence has $N_p = 48$ pulses. (b) The decay time $T_{1/e}$, as a function of the number of pulses N_p for XY4 (solid line), UDD (dotted line), and QDD (dash-dotted line). Solid line shows the scaling relation given by Eq. (18), with T_2 fitted to be 2.73 μs.

both cases, the fidelity decay in UDD is faster than in XY4. The fidelity decay in QDD is even faster than UDD, given that the number of pulses is the same [see Fig. 5(a)]. The $1/e$ decay time of UDD, XY4 (CPMG), and QDD are shown in Fig. 5(b). For all numbers of pulses we have studied, the XY4 sequence performs better than UDD and QDD. Since the noise field $B(t)$ generated by the O-U process has Lorentzian spectral density without sharp cutoff, our results agree with the existing knowledge,[37,49,57–60,62] that for the bath spectrum with a soft cutoff, the pulse sequences with CPMG timing outperform UDD.

V. EFFECTS OF THE PULSE ERROR ACCUMULATION

In this section, we focus on the effect of the pulse error accumulation for the DD sequences introduced above.

A. Model for pulse error description

In our analysis, we assume that the control pulses have infinitely small duration, and, therefore, treat them as rotation operators. The imperfections in the pulses are taken into account by considering the errors in the rotation axis and rotation angles.[44,69,78] For instance, for a nominal π pulse about the x axis (the π_X pulse), the actual evolution of the central spin is expressed as

$$U_X = \exp\left[-i(\pi + \epsilon_x)(\mathbf{S} \cdot \vec{\mathbf{n}})\right], \tag{23}$$

where $\vec{\mathbf{n}} = (\sqrt{1 - n_y^2 - n_z^2}, n_y, n_z)$ is the rotation axis which slightly deviates from the x axis (n_y and n_z are small), and ϵ_x is the error in the rotation angle. Similarly, the rotation operator for a nominally π pulse about the y axis (the π_Y pulse) is

$$U_Y = \exp\left[-i(\pi + \epsilon_y)(\mathbf{S} \cdot \vec{\mathbf{m}})\right], \tag{24}$$

where ϵ_y is the rotation angle error and $\vec{\mathbf{m}} = (m_x, \sqrt{1 - m_x^2 - m_z^2}, m_z)$ is the actual rotation axis.

In the studies below, the pulse errors $\epsilon_x, \epsilon_y, n_y, m_x$ are kept constant for all experimental runs ($\sim 10^6$ in our experiments), and during each single run. This corresponds to an excellent

stability of the pulse-generating hardware used in our experiments. However, the components n_z and m_z or the rotation axes are noticeably affected by the hyperfine coupling $A_0 S^z I_0^z$. Correspondingly, these two errors are treated as static during each run, but have different values for different runs, depending on the values of $I_0^z = 1, 0, -1$ as $n_z = n_0 I_0^z$ and $m_z = m_0 I_0^z$. The parameters taken in the simulation are $\epsilon_x = \epsilon_y = -0.02$, $m_x = 0.005$, $n_0 = m_0 = 0.05$, and $n_y = 0$, being determined from the bootstrap protocol for pulse characterization.[69]

Note that for imperfect pulses, it becomes important how the π rotations are implemented, via π_X or via π_Y pulses. Therefore, in contrast with the previous section, the sequences with the single-axis and with the two-axis control will be considered separately.

B. CPMG sequence

The evolution operator for a period of the CPMG sequence is

$$U^{\mathrm{CPMG}} = U_{\mathrm{d}}(\tau) U_{\mathrm{X}} U_{\mathrm{d}}(\tau) U_{\mathrm{d}}(\tau) U_{\mathrm{X}} U_{\mathrm{d}}(\tau). \tag{25}$$

To gain qualitative insight into the problem of the pulse error accumulation, let us assume that the noise field B is static. Keeping only the terms of the first order in the pulse errors,

$$U^{\mathrm{CPMG}} = -\mathbf{1} + i(\epsilon_x \cos \phi_{\mathrm{d}} + 2n_z \sin \phi_{\mathrm{d}})\sigma^x, \tag{26}$$

where $\phi_{\mathrm{d}} = B\tau$ is the noise phase accumulated during an interpulse delay. For perfect pulses, the evolution operator is identity, and the quantum state of the central spin is preserved perfectly for static noise. For imperfect π_X pulses, the evolution during a CPMG period corresponds to a spin rotation about the x axis by angle $2\pi + \theta_{\mathrm{CPMG}}$ with $\theta_{\mathrm{CPMG}} = -2(\epsilon_x \cos \phi_{\mathrm{d}} + 2n_z \sin \phi_{\mathrm{d}})$. Repeating N_{p} periods, the overall evolution of the central spin is equivalent to a rotation about the same axis by an angle $N_{\mathrm{p}} \theta_{\mathrm{CPMG}}$.

To examine how different spin states are preserved in DD, we study two perpendicular spin components S_{X} and S_{Y}. Since the x component is not affected by rotations about the x axis, the state $|X\rangle$ is preserved very well, being spoiled only by the higher-order terms. For the initial state $|Y\rangle$, in a single realization of B, the y component is

$$S_{Y,\mathtt{single}} = \cos \theta_{\mathrm{CPMG}}, \tag{27}$$

that is, the decoupling fidelity oscillates at a frequency determined by the pulse errors. After averaging $S_{Y,\mathtt{single}}$ over different realizations of B, the fidelity decays due to the pulse error accumulation, as known from the early days of magnetic resonance[52] [i.e., the spin component S_{X} is well preserved in a CPMG sequence, while S_{Y} (when it becomes the CP sequence) is sensitive to the pulse errors ϵ_x and n_z].

To study the experimental case of the dynamical noise [whose parameters are given by Eq. (7)] in the presence of the pulse errors, we performed numerical simulations. The results are shown in Fig. 6 for $N_p = 16$ pulses applied to the states $|X\rangle$ and $|Y\rangle$. The total evolution time is varying from 0 to 15 μs. The simulations agree with the experimental results.

C. Sequences based on PDD XY and XY4

Analysis of the pulse error accumulation for the PDD XY sequence, in the case of static noise, has been carried out in
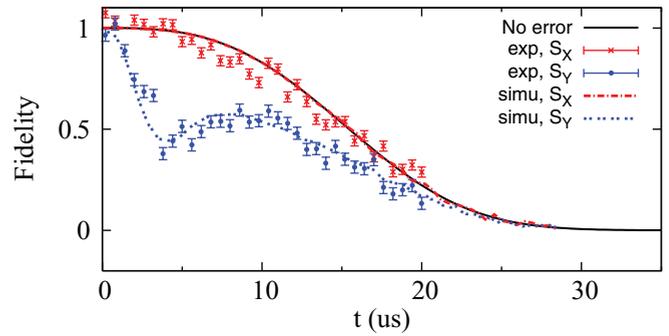
FIG. 6. (Color online) Decoupling fidelity of the CPMG sequence as a function of the total evolution time for initial states $|X\rangle$ (red symbols and lines) and $|Y\rangle$ (blue symbols and lines). The number of pulses is $N_p = 16$. Broken lines are the simulation results; the dots are the experimental results. The black solid line shows the results for ideal pulses.

Ref. 44, and here we only briefly remind the main results. The evolution operator for a single period, to the first order in the pulse errors, is

$$U^{\mathrm{XY}} = -\mathbf{1} - 2i(m_x + n_y)\sigma^z, \tag{28}$$

corresponding to a spin rotation about the z axis by the angle $2\pi + 4(m_x + n_y)$. Thus, only the in-plane components of the rotation axis n_y and m_x accumulate in the course of decoupling. In experiments, these errors can be minimized using appropriate pulse tuning.[65–70] Moreover, in Eq. (28) the evolution operators are independent of ϕ_d, thus being insensitive to the resonance offset, the value of B, and the duration of the interpulse delay, τ.

For the XY4 sequence, in spite of different timing, the pulse errors accumulate in the same way (in the first order in the pulse errors), and the evolution operator for XY4 is also given by Eq. (28) in the case of static noise. Therefore, XY4 is also very robust with respect to most pulse errors. In addition, due to better pulse timing, it demonstrates very good performance in the case of dynamic noise, as shown in Sec. IV. Thus, we expect that this sequence is close to optimal for experiments: It combines simplicity, good scaling properties, and robustness to the pulse imperfections.

Figure 7 shows the decoupling fidelity as a function of the total evolution time for the XY4 sequence with imperfect pulses. The results for the initial states $|X\rangle$ and $|Y\rangle$ with $N_p = 8$ and $N_p = 72$ pulses are shown. Since the in-plane pulse errors in our experiments are very small, XY4 serves as a good decoupling sequence for the NV center spin in a spin bath composed of P1 centers.

The symmetrized version of PDD XY, SDD XY demonstrates worse scaling properties in the case of perfect pulses. However, it has advantages when the pulses are imperfect, as the first-order terms in the pulse errors disappear in the evolution operator. In the case of static noise field, to the second order,

$$U^{\mathrm{SDDXY}} = \mathbf{1} + 2i(m_x + n_y)\epsilon_y \sigma^x$$
$$+ 2i(m_x + n_y)(\epsilon_x \cos \phi_{\mathrm{d}} + 2n_z \sin \phi_{\mathrm{d}})\sigma^y. \tag{29}$$

The evolution operator for the symmetrized version of XY4, the XY8 sequence, has even more symmetric form (again, for
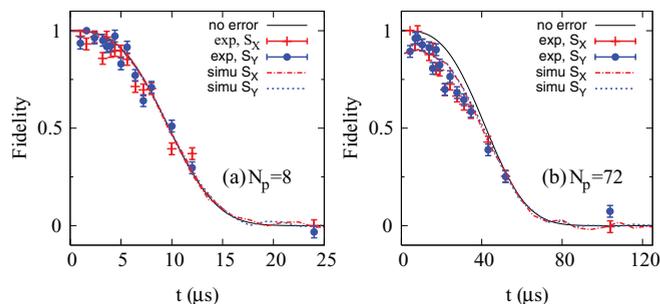
FIG. 7. (Color online) Decoupling fidelity of the XY4 sequence as a function of the total evolution time for the initial states $|X\rangle$ (red symbols and lines) and $|Y\rangle$ (blue symbols and lines), in the presence of the pulse errors. The broken lines are the simulation results, and the dots are the experimental data. The black solid line shows the results for ideal pulses. (a) $N_p = 8$. (b) $N_p = 72$.

static noise):

$$U^{\text{XY8}} = \mathbf{1} + 2i(m_x + n_y)(\epsilon_y \cos\phi_{\text{d}} + 2m_z \sin\phi_{\text{d}})\sigma^x$$
$$+2i(m_x + n_y)(\epsilon_x \cos\phi_{\text{d}} + 2n_z \sin\phi_{\text{d}})\sigma^y. \quad (30)$$

Thus, XY8 presents a good choice for the experimentalist when the pulse errors are not very small: This sequence is still very simple to program, and it has the same good performance as XY4, but is sensitive to the pulse errors only in the second order.

The error accumulation in the concatenated version of PDD XY has been analyzed before.[35,44,56] An important feature is that CDD has an error-correction structure. For the static noise, in the first order, the pulse errors do not accumulate as the concatenation level increases, although the number of pulses increases exponentially. For the concatenated sequences based on XY4, we found that the same feature holds. The evolution operator for $\text{CDD}_\ell^{\text{XY4}}$ is still described by Eq. (28) for any ℓ. While the leading terms are of the first order in the pulse errors, they do not accumulate as the concatenation order or the number of periods increase.

Figure 8 shows the simulation results for the dynamic noise, with the parameters given by Eq. (7), for SDD XY (two periods), CDD_2, XY8 (four periods) and $\text{CDD}_2^{\text{XY4}}$ with pulse number $N_p = 16, 20, 32$, and 36, respectively. Due to
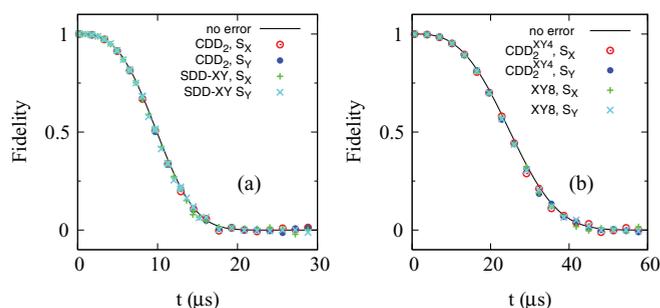
FIG. 8. (Color online) Decoupling fidelity as a function of the total evolution time for initial states $|X\rangle$ and $|Y\rangle$, in the presence of the pulse errors. The results are shown for SDD XY (two periods) and CDD_2 sequences (a), and for XY8 (four periods) and $\text{CDD}_2^{\text{XY4}}$ sequences (b) with the number of pulses $N_p = 16, 20, 32$, and 36, respectively. Black solid line shows the results for ideal pulses.

smallness of m_x and n_y in our simulations, the pulse errors have little effect on the decoupling fidelity, and all sequences perform almost as if there were no pulse errors.

D. UDD and QDD

Since the interpulse delay in UDD is not uniform, we use only the total evolution time T in the following analysis. As above, we present analytical results only for the case of static noise, while the simulations show the results for the dynamical spin bath characterized by Eq. (7).

If the level of UDD is even, $\ell = 2n$, then the pulse number is equal to ℓ. The evolution operator for a single electron spin, to first order in the pulse errors, is

$$U_{2n}^{\text{UDD}} = (-1)^n[\mathbf{1} - i\sigma^x\theta_x], \quad (31)$$

where θ_x is a linear combination of pulse errors ϵ_x and n_z, with coefficients depending on n and BT. The spin is thus rotated about the x axis by an angle $2\theta_x$, which is dependent on ϵ_x and n_z. Comparing to the CPMG sequence analyzed in Sec. V B, we see that for UDD with an even number of the π_X pulses, the spin state $|X\rangle$ is well preserved while the fidelity for the $|Y\rangle$ state is strongly affected by the pulse error accumulation, and the influencing factors are the rotation angle error and the z component of the rotation axis error. Figure 9(a) shows the decoupling performance of UDD_{16} for the dynamical spin bath.

For $\ell = 2n - 1$, the pulse number N_p equals $2n$ (there is a π pulse at the end of the whole evolution). The evolution operator is then

$$U_{2n-1}^{\text{UDD}} = (-1)^n(\mathbf{1} - i\theta_n\sigma^x - i\eta_n\sigma^y), \quad (32)$$

where θ_n and η_n are linear combinations of ϵ_x and n_z, with coefficients depending on n and BT. This operator represents a rotation in the x-y plane, with the axis depending on the relative magnitudes of θ_n and η_n. If $\theta_n \gg \eta_n$, then the axis is closer to the x axis, so that S_X is preserved better than S_Y (and vice versa). We notice that in the limit $T \to 0$, η_n vanishes, hence the pulse error affects S_X at larger times, while S_Y is affected already at small times [see Fig. 9(b)].

In the limit $T \to 0$, in which case the sequence is simply successive pulses, the sequences with $\ell = 2n - 1$ and $\ell = 2n$ are the same, and the evolution operator in the first order
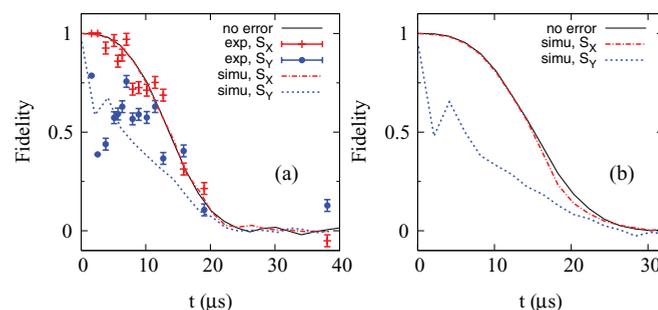
FIG. 9. (Color online) Decoupling fidelity for initial states $|X\rangle$ and $|Y\rangle$ in the presence of pulse errors. Dots and crosses are the experimental data, and the broken and dotted lines are the simulation results for S_X and S_Y, respectively. The solid line shows the simulation results for perfect pulses. (a) UDD_{16}. (b) UDD_{19}.
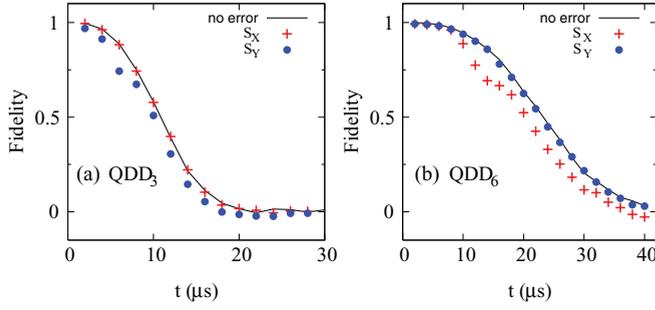
FIG. 10. (Color online) Simulation results. Decoupling fidelity for the initial states $|X\rangle$ (red crosses) and $|Y\rangle$ (blue dots), in the presence of pulse errors. Solid line is the results with ideal pulses. (a) QDD_3. (b) QDD_6.

involves only ϵ_x:

$$\lim_{T \to 0} U_\ell^{\mathrm{UDD}} = (-1)^n (1 - in\epsilon_x \sigma^x), \tag{33}$$

which represents a rotation about the x axis by an angle $2n\epsilon_x$. Hence for UDD sequences of large level, even for small total evolution time, the accumulation of pulse errors in the rotation angle would lead to fidelity loss for the spin state $|Y\rangle$.

Now we consider QDD sequences with π_X pulses in the outer hierarchical level, and π_Y pulses in the inner hierarchical level in the presence of the pulse errors. The sequence of QDD_ℓ with $\ell = 2n - 1$ is shown in Eq. (21) with pulse number $N_p = (\ell + 1)(\ell + 2)$, and for $\ell = 2n$ in Eq. (22) with pulse number $N_p = \ell(\ell + 2)$.

In the limit $T \to 0$, the evolution operators for QDD of even and odd levels are

$$\lim_{T \to 0} U_{2n}^{\mathrm{QDD}} = 1 - in(\epsilon_x \sigma^x + \epsilon_y \sigma^y), \tag{34}$$

$$\lim_{T \to 0} U_{2n-1}^{\mathrm{QDD}} = (-1)^n (1 - in\epsilon_x \sigma^x). \tag{35}$$

That is, for short total evolution time, in a sequence QDD_{2n}, the central spin rotates about an axis lying in the x-y plane. Preservation of the spin states $|X\rangle$ and $|Y\rangle$ is determined by the relative magnitude of ϵ_x, and ϵ_y. If $\epsilon_x \gg \epsilon_y$, then $|X\rangle$ is better preserved, and vice versa. In QDD_{2n-1}, the spin evolution is a rotation about the x axis by an angle $n\epsilon_x$, hence $|Y\rangle$ is better preserved. Note that the rotation axis errors do not contribute in first order to either even or odd level QDD for $T \to 0$. The above features for the initial fidelity loss are seen in Fig. 10, where the simulation results of QDD_3 (with 20 pulses) and QDD_6 (with 48 pulses) are shown for dynamical spin bath. For QDD_3, at short times, $|X\rangle$ is preserved somewhat better than $|Y\rangle$, due to the smallness of ϵ_x in our experiments. For QDD_6, $|X\rangle$ and $|Y\rangle$ exhibit the same behavior at small times, since we have $\epsilon_x = \epsilon_y$.

We did not perform analytical calculations for QDD with finite T since the expansion of the evolution operator is rather cumbersome. Compared to UDD protocol, QDD exhibits much less sensitivity to initial states. In both QDD_3 and QDD_6, the evolutions of S_X and S_Y are close to those with ideal pulses.

To get a comprehensive summary of the behavior of different DD protocols in the presence of pulse errors, Fig. 11 shows the simulation results for (1) XY4 with 12 periods, (2) XY8 with six periods, (3) UDD_{48}, and (4) QDD_6. The number of pulses is 48, the same for each sequence. Since S_X
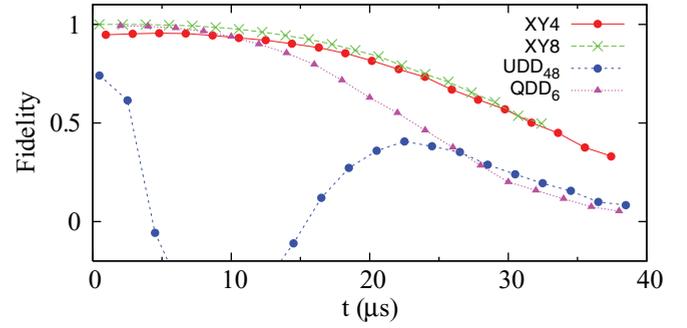
FIG. 11. (Color online) Fidelity S_Y for the $|Y\rangle$ initial state, for different DD sequences in the presence of pulse errors. Results for XY4 (red line and circles), XY8 (green line and crosses), UDD_{48} (blue line and dots), and QDD_6 (magenta line and triangles) are shown. Each sequence contains 48 pulses.

in all cases is only slightly affected by the pulse errors, we plot only the fidelity S_Y to compare different DD protocols. The sequence XY4, which is sensitive to the in-plane rotation axis errors, m_x and n_y, exhibits very small initial decay. Sequence XY8, where the pulse errors are absent in the first order, exhibits no visible effect of the errors, and coincides with the curve for ideal pulses. In the case of UDD based on π_X pulses, the state $|Y\rangle$ is rapidly destroyed by the error accumulation, as expected. In QDD_6, $|Y\rangle$ is little affected by the pulse errors [see Fig. 10(b)], and hence is much better preserved than in UDD_{48}, but its performance in the case of the O-U noise is worse in comparison with XY4 and XY8. Moreover, the leading influencing pulse errors for different DD sequences are summarized in Table I.

As a result, we come to the following conclusion. In the realistic case of the dynamical spin bath (O-U noise) and imperfect pulses, XY4 and XY8 sequences would be the best choices. These two have the same pulse timing, but the accumulation of pulse errors are better suppressed in the latter.

VI. DISCUSSION OF THE INTERNAL STRUCTURE OF THE SPIN BATH COMPOSED OF P1 CENTERS

In the above discussions, we approximated the whole spin bath as a random noise field $B(t)$. A closer examination of the spin bath reveals that, with the static field applied along the symmetry axis of the NV center, the ESR spectrum of the P1 centers is composed of six Lorentzian lines. Thus, the NV center is decohered by six different baths, each one described via its own O-U process. Here we demonstrate that the main conclusions drawn above remain valid.

Each P1 center is composed of an electron spin $S_k = 1/2$ and a nuclear spin $I_k = 1$ (^{14}N nucleus) coupled via hyperfine interaction. The symmetry of this coupling, and the orientation of the nucleus' quadrupolar axis, are determined by the Jahn-Teller distortion at a given P1 location: This distortion reduces the original (local) T_d symmetry of the defect to C_{3v}. Thus, the hyperfine and the quadrupolar Hamiltonians acquire uniaxial symmetry. The symmetry axis is oriented along one of the four $\langle 111 \rangle$ directions in the diamond lattice. But the external static field applied along the [111] axis separates this direction from the other three $\langle 111 \rangle$ axes (which remain equivalent between themselves). Correspondingly, all P1 centers can be

TABLE I. The pulse errors influencing the DD fidelity in the first order for the initial states $|X\rangle$ and $|Y\rangle$, for the corresponding spin components S_X and S_Y.

	CPMG	XY,XY4	UDD[a]	(even ℓ)	(odd ℓ)	QDD($T \to 0$)[b]	(even ℓ)	(odd ℓ)	SDD,XY8	CDD (XY, XY4)
S_X	0	m_x, n_y	0		ϵ_x, n_z		ϵ_x, ϵ_y	0	0	m_x, n_y
S_Y	ϵ_x, n_z	m_x, n_y		ϵ_x, n_z	ϵ_x, n_z		ϵ_x, ϵ_y	ϵ_x	0	m_x, n_y

[a]UDD based on π_X pulses.

[b]QDD with π_X pulses in the outer hierarchical level, and π_Y pulses in the inner hierarchical level.

categorized into two types. Type 1 has its symmetry axis along [111], and type 2 has its symmetry axis along any of [11$\bar{1}$], [1$\bar{1}$1], and [$\bar{1}$11]. The Hamiltonian for a single P1 center of type 1 is[25]

$$\mathcal{H}_{t1} = B_0 S_k^z + A_z S_k^z I_k^z + A_x \left(S_k^x I_k^x + S_k^y I_k^y \right) + P(I_k^z)^2,$$
(36)

where $A_z = 114$ MHz, and $A_x = 81.3$ MHz are the hyperfine couplings along and perpendicular to the symmetry axis of the P1 defect, and $P = -4$ MHz is the quadrupolar coupling constant. The transition frequencies between different pairs of eigenstates for Hamiltonian Eq. (36) can then be calculated. For the static field $B_0 = 114$ Gauss, the flip-flops between S_k and I_k are greatly suppressed, and S_k^z and I_k^z are good approximate quantum numbers. The three main transitions for the electron spin with the frequencies $\nu_{1,3,6} = 217, 339, 441$ MHz correspond to $I_k^z \approx -1, 0, 1$, respectively. Moreover, in this region of external fields, for a P1 center of type 2, the quantization axis is also close to z, and S^z and I^z are again good quantum numbers. The main transitions having noticeable spectral weight, with the frequencies $\nu_{2,4,5} = 249, 347$, and 417 MHz, also take place between the states with approximately the same value of I_k^z.

For a single P1 center spin, all the other surrounding P1 centers can be treated as a spin bath (made of six baths, corresponding to six spectral lines), which create random field along the quantization axis. Taking into account the statistical properties of the dipolar coupling constants,[81,88] one finds that each spectral line of the bath has Lorentian form, and is broadened due to the dipolar interaction between P1 centers by ~ 1 MHz.[99] Each spectral line can be considered as a "spin pocket," and the flip-flops between the electron spins of two P1 centers can happen only if both centers belong to the same pocket (i.e., each spectral line creates its own noise field with rms b_k and the correlation decay rate R_k), with $k = 1, \ldots, 6$. In addition, we can include the quasistatic fluctuations in the applied magnetic field B_0, and describe it as another bath, with rms b_7 and $R_7 = 0$.

The contributions from these independent noise fields to the decay factor are additive, and for the free induction decay and the spin echo we have[81] $F(T) = \exp[-T^2 \sum_{j=1}^{7} b_j^2/2]$ and $E(T = 2\tau) = \exp[-(2\tau)^3 \sum_{j=1}^{6} b_j^2 R_j/12]$, respectively. Similarly, using the results of Sec. IV, for the experimentally optimal sequences XY4 and XY8 (and for the corresponding concatenated protocols) we obtain the DD fidelity,

$$S(T) = \exp\left[-\frac{T^3}{3N_d^2} \sum_{j=1}^{7} b_j^2 R_j\right],$$
(37)

that is, the overall effect of seven independent spin baths is equivalent to a single noise field with the parameters b and R satisfying $b^2 = \sum_{j=1}^{7} b_j^2$ and $b^2 R = \sum_{j=1}^{7} b_j^2 R_j$. In a similar fashion, the main results of Sec. V concerning the influence of the pulse errors, also remain valid for several independent baths.

VII. CONCLUSION

We studied dynamical decoupling (DD) protocols for the nitrogen-vacancy center in diamond, which can be used to decouple the electron spin of the NV center from the spin bath of P1 centers. The decoupling efficiency of various DD schemes is studied, including periodic sequences based on single-axis and double-axis control pulses (CPMG, PDD XY, and XY4), their concatenated and symmetrized versions, as well as aperiodical sequences UDD and QDD.

For the periodical decoupling protocol PDD XY, the fidelity at short times decays 4 times faster than at long times. In the case of the XY4 protocol, the decay rate is uniform at short and long times, and coincides with the slower (long-time) decay rate of PDD XY sequence. For the spin bath under consideration, concatenated and symmetrized versions of the periodic sequences do not improve the decoupling performance, and the aperiodical protocols UDD and QDD exhibit inferior decoupling performance in comparison with XY4.

We also studied the effect of the accumulation of small pulse errors in the course of decoupling. For the DD sequences based on single-axis control (CPMG and UDD), different initial states are affected differently by the imperfect pulses, and are mainly affected by the errors in the rotation angle and the z component of the rotation axis. Thus, the single-axis protocols preserve well only one component of the central spin. For the sequences based on two-axis controls, XY and XY4, the errors associated with the in-plane components of the rotation axes affect the robustness of decoupling in the leading order. In our experimental setup for the decoupling of NV center spin from the P1 centers, such errors are small, ensuring robustness of these protocols, and efficient preservation of all components of the central spin. Similarly, the two-axis QDD protocols are much less sensitive to the pulse errors than their single-axis counterpart UDD.

Overall, for the experimentally relevant case of the dynamical spin bath made of P1 centers, for realistically imperfect pulses, the best choices for an experimentalist are XY4 and XY8 sequences. The former is simpler, but the latter ensures better robustness with respect to the pulse errors. Concatenation does not significantly improve performance, but makes the sequences more complex.

APPENDIX: DERIVATION FOR THE DECAY OF DECOUPLING FIDELITY

We consider a decoupling sequence containing N_c cycles, each of duration T_c (so that $T = N_c T_c$). Each cycle is characterized by the filter function $\xi_0(t)$ defined in Sec. IV A. Expressing $S(T)$ as

$$S(T) = \exp\left[-b^2 W(T)\right], \tag{A1}$$

to calculate the decay exponent $W(T) = \int_0^T ds\, e^{-Rs} p(s)$, we break the domain $[0, T]$ into N_c pieces of length T_c:

$$W(T) = \sum_{m=0}^{N_c - 1} \int_{mT_c}^{(m+1)T_c} e^{-Rs} p(s)\, ds, \tag{A2}$$

and calculate $p(s)$ at each segment $[mT_c, (m+1)T_c]$ separately. Expressing $s = mT_c + s'$ (with $0 < s' < T_c$), and taking into account that $\xi(t)$ and $\xi(t+s)$ overlap over $N_c - m$ full cycles, we have

$$p(s) = (N - m)[q_{11}(s') + q_{12}(s')] - q_{12}(s'), \tag{A3}$$

where

$$q_{11}(s') = \int_0^{T_c - s'} \xi_0(t)\xi_0(t+s')\, dt,$$
$$q_{12}(s') = q_{11}(T_c - s'). \tag{A4}$$

Substitute $p(s)$ into Eq. (A2), using $e^{-Rs} = e^{-mRT_c} e^{-Rs'}$, we obtain

$$W(T) = \Gamma_N \int_0^{T_c} e^{-Rs'}[q_{11}(s') + q_{12}(s')]\, ds'$$
$$- P_N \int_0^{T_c} e^{-Rs'} q_{12}(s')\, ds', \tag{A5}$$

where

$$P_N = \sum_{m=0}^{N_c - 1} e^{-mRT_c},$$
$$\Gamma_N = \sum_{m=0}^{N_c - 1} (N_c - m) e^{-mRT_c}. \tag{A6}$$

Here P_N is a geometric progression and $\Gamma_N = N_c P_N + \frac{1}{T_c}\frac{dP_N}{dR}$. We therefore have

$$P_N = \frac{1 - e^{-N_c RT_c}}{1 - e^{-RT_c}},$$
$$\Gamma_N = \frac{N_c - (N_c + 1)e^{-RT_c} + e^{-(N_c+1)RT_c}}{(1 - e^{-RT_c})^2}. \tag{A7}$$

With the integrals in Eq. (A5) expressed in terms of Q_{11} and Q_{12} defined in Eq. (11), we obtain

$$W(T) = [\Gamma_N(Q_{11} + Q_{12}) - P_N Q_{12}], \tag{A8}$$

and the fidelity decay $S(T)$ is thus simplified to Eq. (10).

The integral Q_{12} can be conveniently calculated from Q_{11} as

$$Q_{12} = e^{-RT_c} \tilde{Q}_{11}, \tag{A9}$$

where $\tilde{Q}_{11}$ denotes replacing R by $-R$ in Q_{11}. This relation will be used repeatedly in the calculations for the fidelity decay of specific pulse sequences.

We now calculate the decay rate $W(t)$ for different DD sequences. focusing on the experimentally interested case $RT_c \ll 1$, and examine behavior at short times $RT \ll 1$, and long times $RT \gg 1$. In theses two limits, constants Γ_N and P_N have expressions,

$$P_N = N_c,$$
$$\Gamma_N = N_c(N_c + 1)/2, \tag{A10}$$

and

$$P_N = 1/(RT_c),$$
$$\Gamma_N = N_c/(RT_c), \tag{A11}$$

respectively.

1. Sequences based on PDD XY

In the sequence of PDD XY, the filter function has a period of $T_c = 2\tau$, and

$$\xi_0(t) = \begin{cases} +1, & \text{for } \tau > t \geqslant 0 \\ -1, & \text{for } 2\tau \geqslant t \geqslant \tau \\ 0, & \text{otherwise.} \end{cases} \tag{A12}$$

Note that the full cycle of the PDD XY sequence, defined according to Ref. 32, is twice longer than the period of the filter function $\xi(t)$. We can take $T_c = 2\tau$, and thus significantly simplify the derivation, because we restrict ourselves to the case of pure dephasing and ideal pulses.

The convolution integral is

$$q_{11}(s) = \begin{cases} 2\tau - 3s, & \text{for } \tau > s \geqslant 0 \\ s - 2\tau, & \text{for } 2\tau > s \geqslant \tau \\ 0, & \text{otherwise.} \end{cases} \tag{A13}$$

The integrals can further be calculated as

$$Q_{11} = \frac{1}{R^2}[2\delta - 3 + 4e^{-\delta} - e^{-2\delta}],$$
$$Q_{12} = \frac{1}{R^2}[-1 + 4e^{-\delta} - (2\delta + 3)e^{-2\delta}], \tag{A14}$$

where $\delta = R\tau$. Focused on the experimentally interested case $\delta \ll 1$, the decay exponent, expanded to order δ^4, is

$$W_{\text{PDD}}(T) = \frac{1}{R^2}\left[\frac{2P_N}{3}\delta^3 + \left(\frac{\Gamma_N}{3} - \frac{5P_N}{6}\right)\delta^4\right]. \tag{A15}$$

At short times, the second term is negligible, and the decay rate becomes

$$W_{\text{PDD}}(T) = \frac{2N_c\delta^3}{3R^2}, \tag{A16}$$

and the fidelity decays as Eq. (12), taking into account that $N_d = 2N_c$ for PDD XY. At long times, the decay rate is found to be

$$W_{\text{PDD}}(T) = \frac{N_c \delta^3}{6R^2}, \tag{A17}$$

resulting in the fidelity decay as Eq. (13).

For the concatenated sequence CDD$_\ell$, consider the filter function for half a period, we found that the integrals Q_{11} and Q_{12} for level ℓ and level $\ell - 1$ are related as

$$Q_{11}^{(\ell)} = \left(2 - e^{-RT_{0c}^{(\ell-1)}}\right) Q_{11}^{(\ell-1)} - Q_{12}^{(\ell-1)}, \tag{A18}$$

where the superscripts denote the concatenation level and $T_{0c}^{(\ell-1)}$ is the duration of the *full* period of CDD$_{\ell-1}$. The other integral, $Q_{12}^{(\ell)}$, can be obtained using Eq. (A9). We now derive the decay exponent for CDD$_\ell$ based on PDD XY. The integrals Q_{11} and Q_{12} for a full period of PDD XY can be obtained from the quantities for half a period to be

$$Q_{11}^{(1)} = \frac{1}{R^2}[-7 + 4\delta + 12e^\delta - 8e^{-2\delta} + 4e^{-3\delta} - e^{-4\delta}],$$

and

$$Q_{12}^{(1)} = \frac{1}{R^2}[-1 + 4e^{-\delta} - 8e^{-2\delta} + 12e^{-3\delta} - (4\delta + 7)e^{-4\delta}].$$

Substituting these result into Eqs. (A18) and (A8), we obtain the decay rate for CDD$_2$. Limiting to the case $RT_c \ll 1$, we find that

$$\begin{aligned} Q_{11}^{(2)} &= \frac{1}{R^2}\left[\frac{8}{3}(RT_c)^3 + o(R^5\tau^5)\right], \\ Q_{12}^{(2)} &= \frac{1}{R^2}\left[\frac{8}{3}(RT_c)^3(-1 + RT_c) + o(R^5\tau^5)\right], \end{aligned} \tag{A19}$$

where $T_c = 8\tau$ for CDD$_2$. Noticing Eqs. (A10) and (A11), we find that for both short times ($N_c RT_c \ll 1$) and for long times ($N_c RT_c \gg 1$) the decay rate is the same, equal to the short-time decay rate of PDD XY, Eq. (A16), taking into account that the half-period of CDD$_2$ is four times as long as the half-period of PDD XY. This analysis can be repeated inductively, in the same manner, for any concatenation level ℓ (starting from CDD$_{\ell-1}$), with the same result.

Note, however, that for CDD, since T_c grows exponentially with ℓ, the condition $RT_c \ll 1$ will be violated for higher-order CDDs, and the corresponding analysis is not applicable anymore. However, for slow baths, the absolute value of the DD fidelity will become only smaller in this case; for fast baths, with $RT_c \gg 1$, DD gives little improvement in any case.

2. Sequences based on XY4

For sequences with CPMG timing, we take $T_c = 4\tau$ and the single-cycle filter function is

$$\xi_0(t) = \begin{cases} +1, & \text{for } \tau > t \geqslant 0 \\ -1, & \text{for } 3\tau > t \geqslant \tau \\ +1, & \text{for } 4\tau > t \geqslant 3\tau \\ 0, & \text{others.} \end{cases} \tag{A20}$$

The convolution integral is then

$$q_{11}(s) = \begin{cases} 4\tau - 5s, & \text{for } \tau > s \geqslant 0 \\ -s, & \text{for } 2\tau > s \geqslant \tau \\ 3s - 8\tau, & \text{for } 3\tau > s \geqslant 2\tau \\ 4\tau - s, & \text{for } 4\tau > s \geqslant 3\tau \\ 0, & \text{others.} \end{cases} \tag{A21}$$

Q_{11} and Q_{12} can be correspondingly calculated as

$$Q_{11} = \frac{1}{R^2}[4\delta - 5 + 4(e^{-\delta} + e^{-2\delta} - e^{-3\delta}) + e^{-4\delta}],$$

$$Q_{12} = \frac{1}{R^2}[1 - 4(e^{-\delta} - e^{-2\delta} - e^{-3\delta}) - (4\delta + 5)e^{-4\delta}].$$

Limiting to the case $\delta \ll 1$, at both short and long times, the decay rate of the fidelity is found to be the same:

$$W_{\text{XY4}}(T) = \frac{4N_c\delta^3}{3R^2}. \tag{A22}$$

Taking into consideration that $N_d = 4N_c$ for XY4, we arrive at the scaling relation Eq. (17).

For concatenated sequence CDD$_\ell^{\text{XY4}}$, taking T_c to be half its period, we found that general relation between integrals for levels ℓ and those for $\ell - 1$ holds as

$$\begin{aligned} Q_{11}^\ell &= \left(4 - e^{-RT_{0c}^{(\ell-1)}} - 2e^{-2RT_{0c}^{(\ell-1)}} + e^{-3RT_{0c}^{(\ell-1)}}\right) Q_{11}^{(\ell-1)} \\ &\quad + \left(-1 - 2e^{-RT_{0c}^{(\ell-1)}} + e^{-2RT_{0c}^{(\ell-1)}}\right) Q_{12}^{(\ell-1)}. \end{aligned} \tag{A23}$$

Starting from XY4, decay rate for any higher level CDD can be derived. Focusing on our interested case $\delta \ll 1$, the integrals for CDD$_\ell^{\text{XY4}}$ is found to be

$$Q_{11} = 8b(R\tau)^3/R^2 + o(R^5\tau^5), \tag{A24}$$

where the terms of order $R^4\tau^4$ are absent, and

$$Q_{12} = 8b(-1 + RT_c)(R\tau)^3/R^2 + o(R^5\tau^5). \tag{A25}$$

Substituting these integrals into Eq. (A8), we find that at both short and long times, the decay rates of CDD$_\ell^{\text{XY4}}$ and CDD$_{\ell-1}^{\text{XY4}}$ are the same, equal to the decay rate of XY4, Eq. (A22), taking into consideration the correct relation between T_c for different concatenation levels.

[1] F. Jelezko, T. Gaebel, I. Popa, M. Domhan, A. Gruber, and J. Wrachtrup, Phys. Rev. Lett. **93**, 130501 (2004).

[2] L. Childress, J. M. Taylor, A. S. Sorensen, and M. D. Lukin, Phys. Rev. Lett. **96**, 070504 (2006).

[3] M. V. G. Dutt *et al.*, Science **316**, 1312 (2007).

[4] P. Cappellaro, L. Jiang, J. S. Hodges, and M. D. Lukin, Phys. Rev. Lett. **102**, 210502 (2009).

[5] L. Jiang *et al.*, Science **326**, 267 (2009).

[6] P. Neumann *et al.*, Nat. Phys. **6**, 249 (2010).

[7] G. D. Fuchs, G. Burkard, P. V. Klimov, and D. D. Awschalom, Nat. Phys. **7**, 789 (2011).

[8] B. B. Buckley, G. D. Fuchs, L. C. Bassett, and D. D. Awschalom, Science **330**, 1212 (2010).

[9] E. Togan *et al.*, Nature (London) **466**, 730 (2010).

[10] L. Robledo, L. Childress, H. Bernien, B. Hensen, P. F. A. Alkemade, and R. Hanson, Nature (London) **477**, 574 (2011)

[11] J. M. Taylor *et al.*, Nat. Phys. **4**, 810 (2008).

[12] G. Balasubramanian *et al.*, Nature (London) **455**, 648 (2008).

[13] J. R. Maze *et al.*, Nature (London) **455**, 644 (2008).

[14] G. de Lange, D. Ristè, V. V. Dobrovitski, and R. Hanson, Phys. Rev. Lett. **106**, 080802 (2011).

[15] F. Dolde *et al.*, Nat. Phys. **7**, 459 (2011).

[16] C. A. Meriles *et al.*, J. Chem. Phys. **133**, 124105 (2010).

[17] L.-S. Bouchard, V. M. Acosta, E. Bauch, and D. Budker, New J. Phys. **13**, 025017 (2011).

[18] L. P. McGuinness *et al.*, Nat. Nanotechnol. **6**, 358 (2011).

[19] J. H. Cole and L. C. L. Hollenberg, Nanotechnology **20**, 495401 (2009).

[20] L. T. Hall, J. H. Cole, C. D. Hill, and L. C. L. Hollenberg, Phys. Rev. Lett. **103**, 220802 (2009).

[21] A. Gruber *et al.*, Science **276**, 2012 (1997).

[22] F. Jelezko *et al.*, Appl. Phys. Lett. **81**, 2160 (2002).

[23] J. Harrison, M. J. Sellars, and N. B. Manson, J. Lumin. **107**, 245 (2004).

[24] L. Childress *et al.*, Science **314**, 281 (2006).

[25] R. Hanson, V. V. Dobrovitski, A. E. Feiguin, O. Gywat, and D. D. Awschalom, Science **320**, 352 (2008).

[26] T. Gaebel *et al.*, Nat. Phys. **2**, 408 (2006).

[27] G. D. Fuchs, V. V. Dobrovitski, D. M. Toyli, F. J. Heremans, and D. D. Awschalom, Science **326**, 1520 (2009).

[28] G. D. Fuchs *et al.*, Nat. Phys. **6**, 668 (2010).

[29] F. Jelezko, T. Gaebel, I. Popa, A. Gruber, and J. Wrachtrup, Phys. Rev. Lett. **92**, 076401 (2004).

[30] C. Santori *et al.*, Phys. Rev. Lett. **97**, 247401 (2006).

[31] P. Tamarat *et al.*, Phys. Rev. Lett. **97**, 083002 (2006).

[32] U. Haeberlen, *High Resolution NMR in Solids: Selective Averaging* (Academic, New York, 1976).

[33] L. Viola and S. Lloyd, Phys. Rev. A **58**, 2733 (1998).

[34] L. Viola, S. Lloyd, and E. Knill, Phys. Rev. Lett. **83**, 4888 (1999).

[35] K. Khodjasteh and D. A. Lidar, Phys. Rev. A **75**, 062310 (2007).

[36] M. J. Biercuk, H. Uys, A. P. Vandevender, N. Shiga, W. M. Itano, and J. J. Bollinger, Nature (London) **458**, 996 (2009).

[37] H. Uys, M. J. Biercuk, and J. J. Bollinger, Phys. Rev. Lett. **103**, 040501 (2009).

[38] L. F. Santos and L. Viola, Phys. Rev. A **72**, 062303 (2005).

[39] G. S. Uhrig, Phys. Rev. Lett. **98**, 100504 (2007); New J. Phys. **10**, 083024 (2008).

[40] G. S. Uhrig, Phys. Rev. Lett. **102**, 120502 (2009).

[41] J. R. West, B. H. Fong, and D. A. Lidar, Phys. Rev. Lett. **104**, 130501 (2010).

[42] H. Bluhm *et al.*, Nat. Phys. **7**, 109 (2011).

[43] J. J. L. Morton *et al.*, Nature (London) **455**, 1085 (2008).

[44] A. M. Tyryshkin *et al.*, e-print arXiv:1011.1903 (to be published).

[45] J. J. L. Morton *et al.*, Nat. Phys. **2**, 40 (2006).

[46] J. Du, X. Rong, N. Zhao, Y. Wang, J. Yang, and R. B. Liu, Nature (London) **461**, 1265 (2009).

[47] C. Barthel, J. Medford, C. M. Marcus, M. P. Hanson, and A. C. Gossard, Phys. Rev. Lett. **105**, 266808 (2010).

[48] E. Fraval, M. J. Sellars, and J. J. Longdell, Phys. Rev. Lett. **95**, 030506 (2005).

[49] G. de Lange, Z. H. Wang, D. Ristè, V. V. Dobrovitski, and R. Hanson, Science **330**, 60 (2010).

[50] C. A. Ryan, J. S. Hodges, and D. G. Cory, Phys. Rev. Lett. **105**, 200402 (2010).

[51] B. Naydenov, F. Dolde, L. T. Hall, C. Shin, H. Fedder, L. C. L. Hollenberg, F. Jelezko, and J. Wrachtrup Phys. Rev. B **83**, 081201(R) (2011).

[52] C. P. Slichter, *Principles of Magnetic Resonance* (Springer, Berlin, 1990).

[53] T. Gullion, D. Baker, and M. S. Conradi, J. Magn. Reson. **89**, 479 (1990).

[54] W. X. Zhang, V. V. Dobrovitski, L. F. Santos, L. Viola, and B. N. Harmon, Phys. Rev. B **75**, 201302(R) (2007); W. Zhang, N. P. Konstantinidis, V. V. Dobrovitski, B. N. Harmon, L. F. Santos, and L. Viola, *ibid.* **77**, 125336 (2008).

[55] L. Viola and E. Knill, Phys. Rev. Lett. **90**, 037901 (2003).

[56] K. Khodjasteh and D. A. Lidar, Phys. Rev. Lett. **95**, 180501 (2005).

[57] L. Cywinski, R. M. Lutchyn, C. P. Nave, and S. Das Sarma, Phys. Rev. B **77**, 174509 (2008).

[58] S. Pasini and G. S. Uhrig, Phys. Rev. A **81**, 012309 (2010).

[59] W. Yang and R.-B. Liu, Phys. Rev. Lett. **101**, 180403 (2008).

[60] L. Cywinski, W. M. Witzel, and S. Das Sarma, Phys. Rev. B **79**, 245314 (2009).

[61] G. A. Alvarez, A. Ajoy, X. Peng, and D. Suter, Phys. Rev. A **82**, 042306 (2010).

[62] M. J. Biercuk, H. Uys, A. P. VanDevender, N. Shiga, W. M. Itano, and J. J. Bollinger, Phys. Rev. A **79**, 062324 (2009).

[63] D. Hayes, K. Khodjasteh, L. Viola, and M. J. Biercuk, Phys. Rev. A **84**, 062323 (2011).

[64] B. C. Gerstein and C. R. Dybowski, *Transient Techniques in NMR of Solids* (Academic Press, Orlando, 1985).

[65] J. J. L. Morton, A. M. Tyryshkin, A. Ardavan, K. Porfyrakis, S. A. Lyon, and G. A. D. Briggs, Phys. Rev. A **71**, 012332 (2005).

[66] D. P. Burum, M. Linder, and R. R. Ernst, J. Magn. Reson. **43**, 463 (1981).

[67] A. J. Shaka, D. N. Shykind, G. C. Chingas, and A. Pines, J. Magn. Reson. **80**, 96 (1988).

[68] N. Khaneja, T. Reiss, C. Kehlet, T. Schulte-Herbrüggen, and S. J. Glaser, J. Mag. Res. **172**, 296 (2005).

[69] V. V. Dobrovitski, G. de Lange, D. Ristè, and R. Hanson, Phys. Rev. Lett. **105**, 077601 (2010).

[70] E. M. Fortunato, M. A. Pravia, N. Boulant, G. Teklemariam, T. F. Havel, and D. G. Cory, J. Chem. Phys. **116**, 7599 (2002).

[71] N. Boulant, K. Edmonds, J. Yang, M. A. Pravia, and D. G. Cory, Phys. Rev. A **68**, 032305 (2003).

[72] P. Sengupta and L. P. Pryadko, Phys. Rev. Lett. **95**, 037202 (2005).

[73] M. H. Levitt, J. Magn. Reson. **48**, 234 (1982); Prog. NMR Spectroscopy **18**, 61 (1986).

[74] A. M. Souza, G. A. Alvarez, and D. Suter, Phys. Rev. Lett. **106**, 240501 (2011).

[75] A. J. Shaka and J. Keeler, Prog. NMR Spectr. **19**, 47 (1987).

[76] Z.-H. Wang and V. V. Dobrovitski, J. Phys. B **44**, 154004 (2011).

[77] K. Khodjasteh, V. V. Dobrovitski, and L. Viola, Phys. Rev. A **84**, 022336 (2011).

[78] Z.-H. Wang, W. Zhang, A. M. Tyryshkin, S. A. Lyon, J. W. Ager, E. E. Haller, and V. V. Dobrovitski, Phys. Rev. B **85**, 085206 (2012).

[79] J. Wrachtrup and F. Jelezko, J. Phys.: Condens. Matter **18**, S807 (2006).

[80] B. Smeltzer, J. McIntyre, and L. Childress, Phys. Rev. A **80**, 050302(R) (2009).

[81] J. R. Klauder and P. W. Anderson, Phys. Rev **125**, 912 (1962).

[82] R. Kubo, M. Toda, and N. Hashitsume, *Statistical Physics II* (Springer, Berlin, 1998).

[83] P. Hu and S. R. Hartmann, Phys. Rev. B **9**, 1 (1974).

[84] K. M. Salikhov, S. A. Dzuba, and A. M. Raitsimring, J. Magn. Reson. **42**, 255 (1981).

[85] V. V. Dobrovitski, A. E. Feiguin, R. Hanson, and D. D. Awschalom, Phys. Rev. Lett. **102**, 237601 (2009).

[86] R. de Sousa and S. Das Sarma, Phys. Rev. B **68**, 115322 (2003).

[87] W. M. Witzel, R. de Sousa, and S. Das Sarma, Phys. Rev. B **72**, 161306(R) (2005).

[88] V. V. Dobrovitski, A. E. Feiguin, D. D. Awschalom, and R. Hanson, Phys. Rev. B **77**, 245212 (2008).

[89] S. K. Saikin, Wang Yao, and L. J. Sham, Phys. Rev. B **75**, 125314 (2007).

[90] Ren-Bao Liu, Wang Yao, and L. J. Sham, New J. Phys. **9**, 226 (2007).

[91] J. R. Maze, J. M. Taylor, and M. D. Lukin, Phys. Rev. B **78**, 094303 (2008).

[92] W. M. Witzel, M. S. Carroll, A. Morello, L. Cywinski, and S. Das Sarma, Phys. Rev. Lett. **105**, 187602 (2010).

[93] E. Barnes, L. Cywinski, and S. Das Sarma, Phys. Rev. B **84**, 155315 (2011).

[94] W. A. Coish and J. Baugh, Phys. Status Solidi B **246**, 2203 (2009).

[95] W. A. Coish and D. Loss, Phys. Rev. B **70**, 195340 (2004).

[96] W. X. Zhang, N. Konstantinidis, K. A. Al-Hassanieh, and V. V. Dobrovitski, J. Phys.: Condens. Matter **19**, 083202 (2007).

[97] N. G. van Kampen, *Stochastic Processes in Physics and Chemistry* (Elsevier, Amsterdam, 1981).

[98] M. A. Nielsen and I. L. Chuang, *Quantum Computations and Quantum Information* (Cambridge University Press, Cambridge, 2002).

[99] G. de Lange, T. van der Sar, M. S. Blok, Z.-H. Wang, V. V. Dobrovitski, and R. Hanson, e-print arXiv:1104.4648 (to be published).

[100] A. Abragam, *Principles Of Nuclear Magnetism* (Clarendon, Oxford, 1961).